ORIGINAL ARTICLE

WILEY Cell Proliferation

Topographical cues of direct metal laser sintering titanium surfaces facilitate osteogenic differentiation of bone marrow mesenchymal stem cells through epigenetic regulation

Guoying Zheng[1,2] | Binbin Guan[3] | Penghui Hu[1] | Xingying Qi[1] | Pingting Wang[4] | Yu Kong[2] | Zihao Liu[1] | Ping Gao[1] | Rui Li[2] | Xu Zhang[4] | Xudong Wu[2] | Lei Sui[1]

[1]Department of Prosthodontics, Tianjin Medical University School and Hospital of Stomatology, Tianjin, China

[2]Department of Cell Biology, 2011 Collaborative Innovation Center of Tianjin for Medical Epigenetics, Tianjin Key Laboratory of Medical Epigenetics, Tianjin Medical University, Tianjin, China

[3]Department of Stomatology, Tianjin Medical University General Hospital, Tianjin, China

[4]Department of Endodontics, Tianjin Medical University School and Hospital of Stomatology, Tianjin, China

Correspondence
Xudong Wu, Department of Cell Biology, 2011 Collaborative Innovation Center of Tianjin for Medical Epigenetics, Tianjin Key Laboratory of Medical Epigenetics, Tianjin Medical University, Tianjin, China.
Email: wuxudong@tmu.edu.cn
and
Lei Sui, Department of Prosthodontics, Tianjin Medical University School and Hospital of Stomatology, Tianjin, China.
Email: suilei@tmu.edu.cn

Abstract

Objectives: To investigate the role of hierarchical micro/nanoscale topography of direct metal laser sintering (DMLS) titanium surfaces in osteogenic differentiation of bone marrow mesenchymal stem cells (BMSCs), as well as the possible underlying epigenetic mechanism.

Materials and methods: Three groups of titanium specimens were prepared, including DMLS group, sandblasted, large-grit, acid-etched (SLA) group and smooth titanium (Ti) group. BMSCs were cultured on discs followed by surface characterization. Cell adhesion and proliferation were examined by SEM and CCK-8 assay, while osteogenic-related gene expression was detected by real-time RT-PCR. Immunofluorescence, western blotting and *in vivo* study were also performed to evaluate the potential for osteogenic induction of materials. In addition, to investigate the underlying epigenetic mechanisms, immunofluorescence and western blotting were performed to evaluate the global level of H3K4me3 during osteogenesis. The H3K4me3 and H3K27me3 levels at the promoter area of the osteogenic gene *Runx2* were detected by ChIP assay.

Results: The DMLS surface exhibits greater protein adsorption ability and shows better cell adhesion performance than SLA and Ti surfaces. Moreover, both *in vitro* and *in vivo* studies demonstrated that the DMLS surface is more favourable for the osteogenic differentiation of BMSCs than SLA and Ti surfaces. Accordingly, osteogenesis-associated gene expression in BMSCs is efficiently induced by a rapid H3K27 demethylation and increase in H3K4me3 levels at gene promoters upon osteogenic differentiation on DMLS titanium surface.

Conclusions: Topographical cues of DMLS surfaces have greater potential for the induction of osteogenic differentiation of BMSCs than SLA and Ti surfaces both *in vitro* and *in vivo*. A potential epigenetic mechanism is that the appropriate topography allows rapid H3K27 demethylation and an increased H3K4me3 level at the promoter region of osteogenesis-associated genes during the osteogenic differentiation of BMSCs.

wileyonlinelibrary.com/journal/cpr

1 | INTRODUCTION

Generally, the surface of intraosseous implants could be considered as stem cell niche that instructs stem cells to either self-renew or differentiate.[1,2] In this local environment, stem cell fate is well known to be controlled by genetic and biochemical mediators. However, increasing evidence has revealed that biophysical properties of the surface, particularly topographical cues, also have substantial influence on cellular behaviours.[3,4] Previous studies have shown that the topographical features of implant surfaces, such as scale (micro- or nano-), type (grooves, pits or ridges) and distribution (random or ordered), regulate the adhesion, proliferation and differentiation of bone marrow mesenchymal stem cells (BMSCs),[5-11] and consequently affect the commencement and outcome of osseointegration which is a prerequisite for long-term success of intraosseous implants. Therefore, appropriate topographical features of implant surfaces should be constructed to facilitate the differentiation of BMSCs into the osteogenic lineage to eventually obtain the desired osseointegration.

Direct metal laser sintering (DMLS), one of the latest 3D printing techniques, can be used to fabricate custom-made intraosseous implants with required microscale surface structures. In this technique, implants with a defined complex geometrical structure and shape are built layer by layer from titanium alloy powder on the basis of a virtual 3D model.[12] Together with acid-etching process, DMLS technique could conveniently provide a specific rough surface with hierarchical micro/nanoscale topography, which mimics the natural bone structure assembled from microscale collagen fibres and nanoscale hydroxyapatite crystals.[13-15] Implant surfaces with hybrid or hierarchical micro/nanostructures have been shown to outperform those with individual microscale or nanoscale topography in new bone tissue formation.[16-23] Therefore, DMLS titanium surface is considered a promising intraosseous implant surface candidate, and it is tempting to evaluate the BMSC response to this surface, as well as to further investigate the underlying mechanism.

The mechanism of stem cell differentiation varies widely both in temporal and spatial dimensions, in which dynamic post-translational modifications at the N-terminal tails of nucleosomal histones have been widely implicated in and are thought to be essential in regulating chromatin functions.[24,25] For example, the precise control of the trimethylation levels of histone H3 at lysine 4 (H3K4me3) and H3 at lysine 27 (H3K27me3) at gene promoters is crucial to tip the balance towards gene activation or repression.[26] Several studies have indicated that topographical cues influence the epigenetic signature and function of stem cells by increasing the global levels of histone H3 acetylation.[24,27] Therefore, understanding how the hierarchical micro/nanostructure of DMLS surface affects chromatin modifications and gene transcription would be of great significance.

Herein, we hypothesized that DMLS surface with hierarchical micro/nanoscale topography could facilitate osteogenic differentiation of BMSCs through regulating the co-occupancy and dynamics of H3K4me3 and H3K27me3 at gene promoters. DMLS surfaces were fabricated and characterized. BMSC response to DMLS surface was investigated with sandblasted, large-grit, acid-etched (SLA) titanium surface and smooth titanium surface as control. Furthermore, global level of H3K4me3 during osteogenesis was evaluated, while the H3K4me3 and H3K27me3 levels at the promoter area of the osteogenesis-associated gene *Runx2* were detected. Our results showed that the hierarchical micro/nanoscale topography of DMLS surface promotes the osteogenic differentiation of BMSCs both *in vitro* and *in vivo*. Mechanistically, the hierarchical micro/nanoscale topography leads to H3K27 demethylation and increased levels of H3K4me3 at the promoter of the *Runx2* gene.

2 | MATERIALS AND METHODS

2.1 | Specimen preparation

Three groups of titanium specimens (disc-shaped, 10-mm diameter and 1-mm thickness, Ti-6Al-4V; Institute of Aeronautical Materials, Beijing, China) were prepared, including DMLS group, SLA group and smooth titanium (Ti) group. DMLS discs (particle size 15-45 μm) were fabricated in an argon atmosphere with Yb fibre laser system (EOS M280, EOS GmbH, Krailling, Germany) using a wavelength of 1054 nm, continuous power of 200 W, scanning speed of 7 m/s and a laser spot size of 0.1 mm. The resultant discs were then etched with 1.5% HF for 12 minutes to generate surfaces with hierarchical micro/nanostructure. Smooth Ti discs were polished with silicon carbide sandpaper of No. 240, 360, 400, 600, 800, 1000 and 2000 grits in series. The SLA discs were prepared by sandblasting and acid-etching technology. To remove residual impurities after the fabrication process, all the specimens were immersed in NaOH (20 g/L) and hydrogen peroxide (20 g/L) at 80°C for 30 minutes and then ultrasonically washed with acetone, absolute alcohol and Milli-Q water sequentially. Finally, specimens were cleaned with double-distilled water (ddH$_2$O) in an ultrasonic cleaner for 30 minutes, dried at room temperature for 1 hour and sterilized in an autoclave at 120°C for 20 minutes before use.

2.2 | Surface characterization

SEM (*SUPRA* 55 SAPPHIRE, Oberkochen, Germany) was used to observe surface morphology of specimens. High-magnification images were used to qualitatively evaluate the surface nanoscale features. Drop contact angle measurements were performed with both simulated body fluid (SBF) and ddH$_2$O to assess the wettability. Protein adsorption assays were performed by culturing 100 mg/mL of FITC-BSA (Solarbio, Beijing, China) for 30 minutes on the specimens and samples being viewed under a fluorescence microscope (Olympus, Tokyo, Japan).

2.3 | BMSC culture and osteogenic induction

BMSCs (Purchased from Peking Union Medical College, China) were cultured in fresh DMEM (HyClone, Logan, UT, USA) with

10% FBS (Gibco, New York, NY, USA) and 1% penicillin/strepto-mycin and incubated in a 5% CO_2 atmosphere at 37°C. BMSCs were seeded at a density of 1×10^4 cells/well and incubated on specimens. Culture medium was replaced the next day with oste-oinduction (OI) medium containing 10% FBS, 1% penicillin/strep-tomycin, 50 µg/mL ascorbic acid, 10 nmol/L dexamethasone and 5 mmol/L β-glycerophosphate. The medium was changed every 3 days. Samples were cultured for the desired times in the follow-ing experiments.

2.4 | BMSC adhesion assay and morphological observation

After 6 and 24 hours of culture, samples were fixed in 4% glutaral-dehyde, blocked with BSA and stained with rhodamine-phalloidin (Sigma-Aldrich, St. Louis, MO, USA) and DAPI (Sigma-Aldrich) sequen-tially. F-actin and cell nuclei were visualized under a confocal laser scanning microscope (CLSM) (SP8, Germany). To observe cell mor-phology, samples were dehydrated in a graded ethanol series after being fixed, dried and deposited with a 10-nm-thick gold-palladium. The morphology of the attached cells was examined using SEM.

2.5 | BMSC proliferation assay

At certain time points, cells attached to specimens were incubated with Cell Counting Kit-8 (CCK-8, Dojindo, Japan) reagent. Relative cell number was determined by measuring the absorbance at 450 nm and calculating the OD values to construct growth curves. To visu-ally determine the number of cells for each sample, dual fluorescence staining solution (10 µL) containing 100 µg/mL AO and 100 µg/

TABLE 1 Primer sequences for real-time PCR

| Gene	Primer sequences (5′-3′)
RUNX2	F: AACGATCTGAGATTTGTAGGC
	R: CGGTCAGAGAACAAACTAGG
OC	F: GCCGGAGTCTGTTCACTACC
	R: GCGCTCTGTCTCTCTGACCT
GAPDH	F: CGTCTTCACCACCATGGAGA
	R: CGGCCATCACGCCAGTTT

mL EB (AO/EB, Sigma, USA) was added to each well after 1, 3, 5 and 7 days of culture. After 5 minutes, all the samples were viewed under a fluorescence microscope.

2.6 | Alkaline phosphatase activity analysis

Bone marrow mesenchymal stem cells were seeded at the same den-sity, cultured with and without OI on Ti, SLA and DMLS surfaces. After 7 and 14 days, cells were collected, sonicated and centrifuged. Cell lysate aliquots were collected to evaluate alkaline phosphatase (ALP) activity using an alkaline phosphatase ELISA kit (Solarbio). The total protein content was measured using a BCA kit (Bio-Rad, CA, USA). ALP levels were normalized to the total protein content.

2.7 | qRT-PCR analysis

After 7 and 14 days of culture with specimens, total cellular RNA was extracted using TRIzol (Gibco). The primers for the osteogenesis-related genes Runx2 and OC are listed in Table 1. The
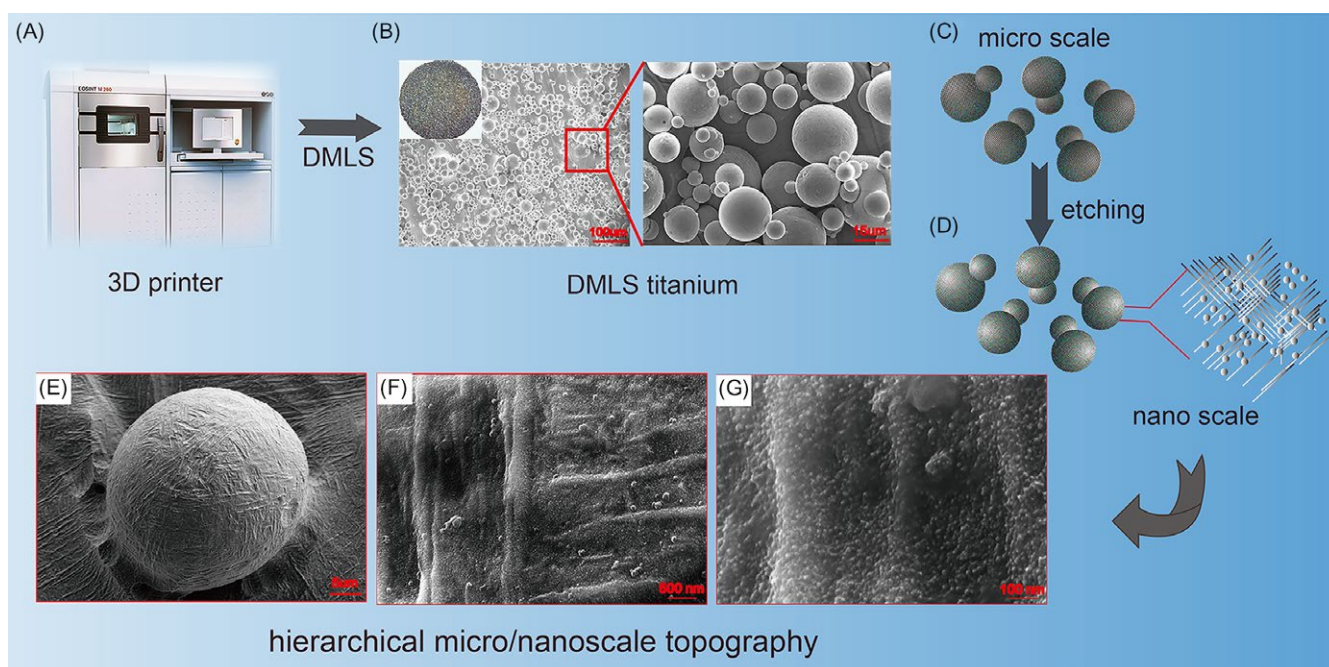
FIGURE 1 Scheme showing the surface of etched DMLS titanium with hierarchical micro- (spherical microparticles) and nanotopography (grooves and nanoparticles) fabricated by a combined DMLS and etching process

qRT-PCR analysis was performed on an Applied Biosystems 7500 system using a QuantiTect SYBR Green PCR Kit (Qiagen, Hilden, Germany). Housekeeping gene *GAPDH* was used to normalize the gene expression.[28.]

2.8 | Immunofluorescence

After 7 and 14 days of culture, the samples were fixed in 4% para-formaldehyde, permeabilized with 0.05% Triton X-100 (Sigma-Aldrich) and then blocked in BSA solution. The primary antibodies were rabbit anti-*Runx2* antibody (Abcam, Cambridge, MA, USA) and rabbit anti-tri-H3K4-methylation antibody (Cell Signalling Technology, Bevery, MA, USA). The secondary antibody was a rhodamine-conjugated anti-rabbit antibody (Invitrogen, Carlsbad, CA, USA).

2.9 | Ectopic bone formation *in vivo*

The protocol and procedures employed were ethically reviewed and approved by the Animal Ethical and Welfare Committee. The BMSCs were cultured on discs for 7 days *in vitro* with or without OI. Then, BMSC-coated discs were implanted into back muscle pockets of Sprague Dawley rats. At 6 and 8 weeks after surgery, the implants were harvested together with surrounding tissues. The samples were fixed, dehydrated, embedded in resin and then sectioned. After HE and toluidine blue (TB) staining, the slices were observed under a fluorescence microscope.

2.10 | Chromatin immunoprecipitation assays

The chromatin immunoprecipitation (ChIP) assay was performed as previously described.[29] Briefly, at specified time points during OI, BMSCs cultured on the SLA and DMLS surfaces were cross-linked in 1% formaldehyde for 8 minutes at 37°C. Non-specific rabbit IgG and H3K4me3 or H3K27me3 antibodies (Cell Signalling Technology) were incubated with Protein G beads (Invitrogen) at 4°C for 2 hours. These antibody-bead complexes were then im-munoprecipitated with DNA fragments for 12 hours at 4 °C. The precipitated DNA was amplified using real-time PCR. The
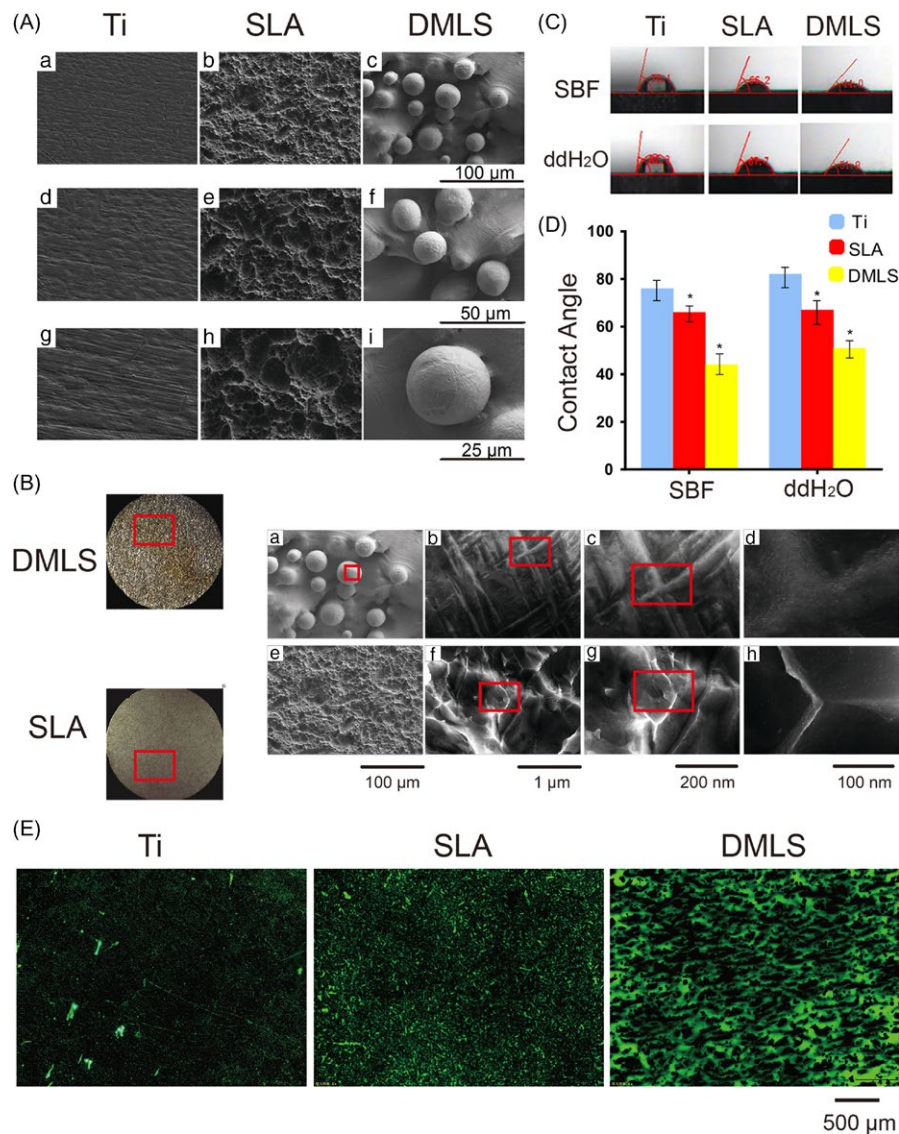
FIGURE 2 Surface characterization of Ti, SLA and etched DMLS titanium discs. (A) SEM observation of Ti, SLA and etched DMLS titanium surface at 500×, 1000× and 2000× magnification. (B) SEM observation of SLA and etched DMLS titanium surface at 500×, 10 000×, 50 000× and 100 000× magnification. (C) Photographs of the contact angle measurement in SBF and ddH$_2$O. (D) Contact angle in SBF and ddH$_2$O. Error bars represent SD (n = 3). *P < .05. (E) FITC-BSA adsorption on Ti, SLA and DMLS titanium after 2 h of incubation

primer pair used was that for *Runx2* promoter (region +540 to +639): (forward) 5′-GCCCTGATCTTCTTACCCCG-3′ and (reverse) 5′-AGTGAACGAGCAAGGGAACC-3′.

2.11 | Western blot analysis

After 14 days of OI, BMSCs cultured on Ti, SLA and DMLS surfaces were collected, sonicated and then centrifuged. The proteins in the supernatant were transferred to PVDF membranes. The membranes were blocked, incubated with anti-Runx2 antibody (Abcam) and anti-H3K4me3 antibody (Cell Signalling Technology) overnight, and incubated with secondary antibody for 1 hour the next day. Finally, the membranes were exposed using an ECL kit (CWBIO, Beijing, China) to visualize the immunoreactive protein bands.

2.12 | Statistical analysis

All experiments were repeated at least 3 times to ensure the validity of observations, and all values are expressed as the mean ± standard deviation (SD). The data were tested for homogeneity and then assessed using one-way ANOVA and the least significant difference test. Error bars represent SD (n = 3). $P < .05$ was considered

significant, and $P < .01$ was considered highly significant (*$P < .05$, **$P < .01$).

3 | RESULTS

3.1 | Characterization of DMLS titanium surfaces

The fabrication process and resultant titanium disc surfaces with the hierarchical micro/nanoscale topography of DMLS titanium are schematically presented in Figure 1. As observed by SEM, the topography of the DMLS titanium surface is composed of randomly dispersed interconnected spherical microparticles (Figure 1B,C). The average diameter of the microparticles is about 25 μm, with a range of approximately 15-45 μm (Figure 2A). As shown in Figures 1D-G and 2B, hierarchical micro/nanoscale structures (micro- or nanogrooves and nanoparticles) are apparent on the surfaces of the microparticles after etching. By contrast, no grooves or particles are observed at the nano-level on the SLA surface (Figure 2Bh).

Drop contact angle measurements with ddH₂O and SBF showed that the contact angles on the DMLS surface are smaller than those on the SLA and Ti surfaces ($P < .05$) (Figure 2C,D), indicating that DMLS surface is more hydrophilic than SLA and Ti surfaces.
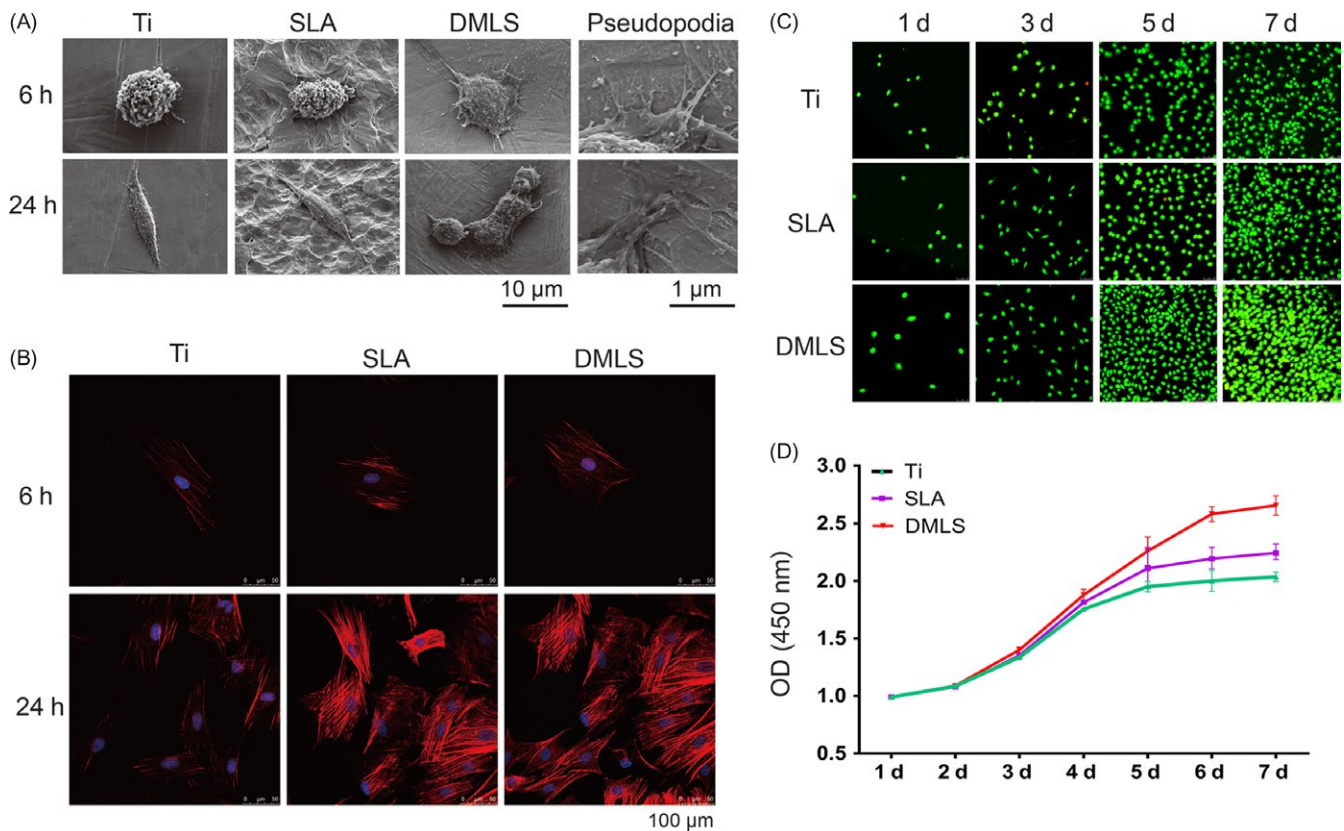
FIGURE 3 BMSC adhesion and proliferation on different titanium surfaces. (A) SEM observation of BMSCs on Ti, SLA and direct metal laser sintering (DMLS) titanium surfaces after 6 and 24 h of seeding. Pseudopodia of BMSCs extending on the DMLS titanium surface were observed. (B) CLSM images of BMSCs (red, cytoskeleton; blue, DAPI) on Ti, SLA and DMLS titanium surfaces after 6 and 24 h of seeding. (C) AO-EB staining images of BMSCs on Ti, SLA and DMLS titanium surfaces after 1, 3, 5 and 7 days of seeding. (D) Growth curves of BMSCs on Ti, SLA and DMLS titanium surfaces

FITC-BSA adsorption assays revealed that DMLS surfaces had the largest amount of protein aggregates among the 3 surfaces, suggesting that DMLS surface has greater protein adsorption ability than the SLA and Ti surfaces (Figure 2E).

3.2 | BMSC adhesion and proliferation

To quantify cell adhesion, SEM and CLSM imaging were performed to view both the morphology and number of adhered BMSCs on 3 different titanium surfaces, 6 and 24 hours after seeding. As shown in Figure 3A, the cells spread well and extended with long pseudopodia on the DMLS surface. By contrast, the cell pseudopodia were less extended on the Ti and SLA surfaces. CLSM images (Figure 3B) revealed the fewest cells on the Ti surfaces but no significant differences in cell number on the SLA and DMLS titanium surfaces.

As shown in Figure 3C, the cell numbers on the 3 different surfaces were comparable at 1 and 3 days, but a larger amount of cells

were observed on the DMLS surface at 5 and 7 days. The growth curves (Figure 3D) of 3 groups were all logarithmic. However, BMSC proliferation on the SLA and Ti surfaces reached a plateau on the 5th day, whereas the cells on the DMLS surfaces continued to grow and did not reach a proliferation plateau until day 6 of culture.

3.3 | Osteogenic differentiation of BMSCs on DMLS titanium surfaces

After 7 days of culture, ALP activity in DMLS group was higher than that in the other groups with or without OI ($P < .05$). On the 14th day, ALP activity was more sharply increased in the DMLS group ($P < .01$) (Figure 4A). In addition, relative expression of the osteogenesis-related genes *Runx2* and *OC* in BMSCs on DMLS surfaces was higher than that on the SLA and Ti surfaces after 7 and 14 days of culture (Figure 4B,C). Furthermore, immunofluorescence data showed that cells on DMLS specimens with OI had the strongest Runx2-positive staining compared with that of other groups (Figure 4D). Additionally,
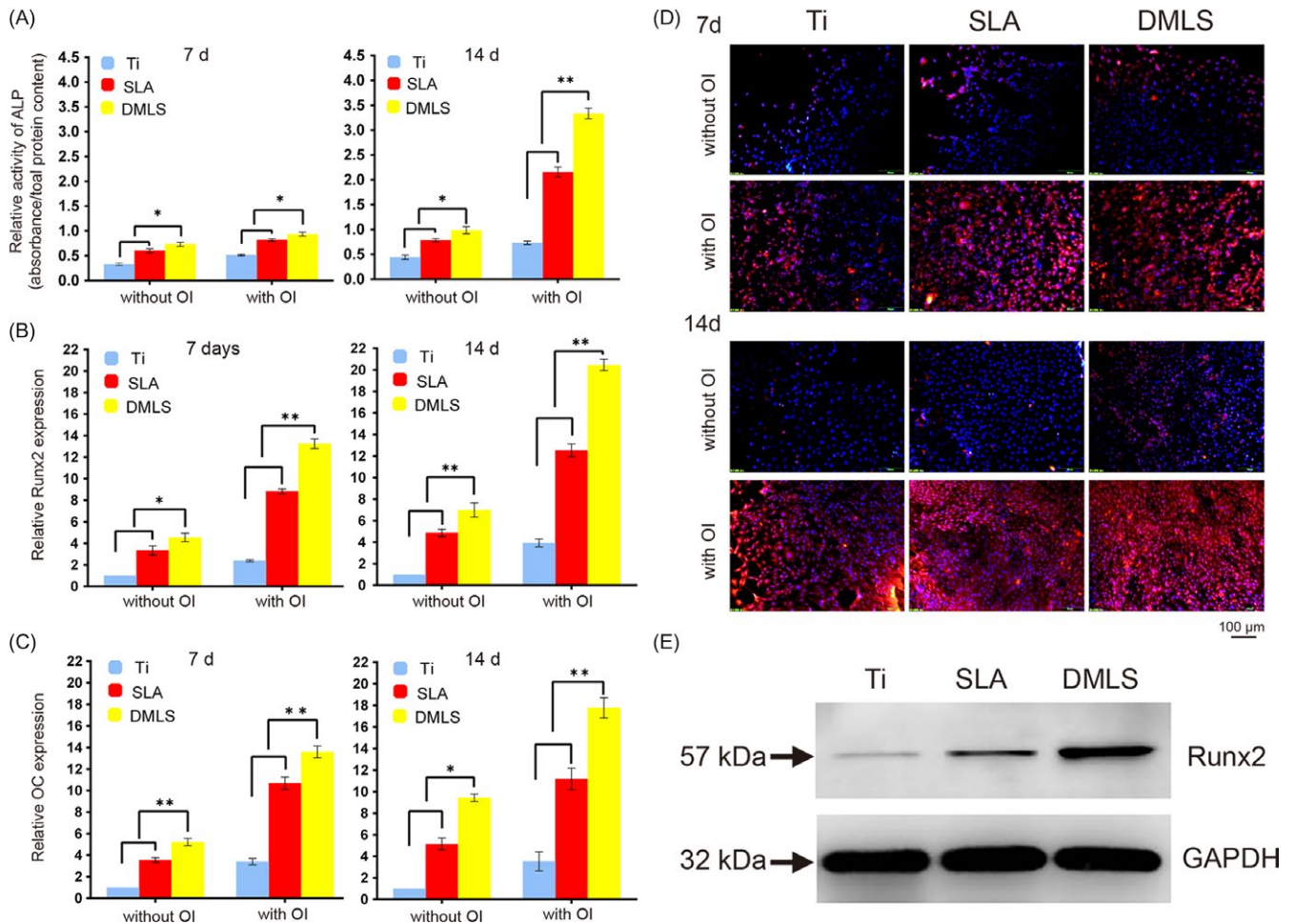
FIGURE 4 Osteogenic differentiation of BMSCs on titanium surfaces *in vitro*. (A) ALP activity of BMSCs cultured on Ti, SLA, and direct metal laser sintering (DMLS) titanium surfaces for 7 and 14 days. (B) The relative mRNA levels of *Runx2* in BMSCs cultured in the designated conditions on different materials for 7 and 14 days. (C) The relative mRNA levels of *OC* in BMSCs cultured according to the different groups for 7 and 14 days. (D) Immunofluorescence staining assays for Runx2 in BMSCs (red, Runx2; blue, DAPI) cultured on different samples for 7 and 14 days. (E) The total protein expression of Runx2 in BMSCs at 14 days after osteoinduction was examined by western blot. Error bars represent SD (n = 3). *$P < .05$. **$P < .01$

the total Runx2 protein level in the DMLS group was higher than that in the Ti and SLA groups, as examined by western blot (Figure 4E).

3.4 | Ectopic bone formation *in vivo*

HE was used to stain the bone matrix as a uniform acidophilic tissue. Uniform dark blue staining by TB confirmed formation of the bone matrix. Only bone tissue showing both positive HE staining and TB staining was considered to demonstrate actual bone formation. Six weeks after implantation, obvious bone matrix formation was observed on the DMLS surfaces. By contrast, muscle tissues with large amounts of spindle-like cells were observed on the Ti and SLA surfaces. Notably, the neo-bone matrix invaded into the pore regions of the DMLS specimen with no noticeable foreign body reaction or inflammatory reaction. Eight weeks after implantation, ectopic bone formation was more significant on the DMLS titanium surface, and the number of cells in the bone matrix decreased (Figure 5).

3.5 | Epigenetic regulation of *Runx2* in BMSCs via DMLS surface topography

To investigate the mechanism of topographical cues of DMLS surface in promoting osteogenic differentiation of BMSCs, global levels of H3K4me3 were measured by western blot and immunostaining

assays. After 7 and 14 days of OI, a marked increase in H3K4me3 levels was detected in the cells cultured on DMLS surfaces compared with the levels in the SLA group (Figure 6A,B).

Chromatin immunoprecipitation assay demonstrated a bivalent state with co-occupancy by the H3K4me3 and H3K27me3 markers at the *Runx2* promoter in BMSCs before OI (Figure 6C). Upon induction of BMSC differentiation, the levels of H3K27me3 at the *Runx2* promoter rapidly and sharply decreased at day 1, especially in the DMLS group. By contrast, the H3K4me3 level at the *Runx2* promoter markedly increased at 7 and 14 days of OI, especially in the DMLS group (Figure 6C,D).

4 | DISCUSSION

The topographical features of material surface are known to modulate the adsorption and conformation of extracellular matrix (ECM) proteins, and adsorbed ECM proteins act as extracellular ligands to specifically bind to cell receptors and mediate cell adhesion.[30-33] Thus, protein adsorption is the very first biological event of cell-material interactions. Generally, protein adsorption is affected by a range of surface properties, especially hydrophilicity and topography.[33-35] For example, Ko et al[36] reported that a hydrophilic surface could strengthen the binding of adhesion proteins to the surface. De et al[37] reported that fibronectin in medium selectively adsorbs
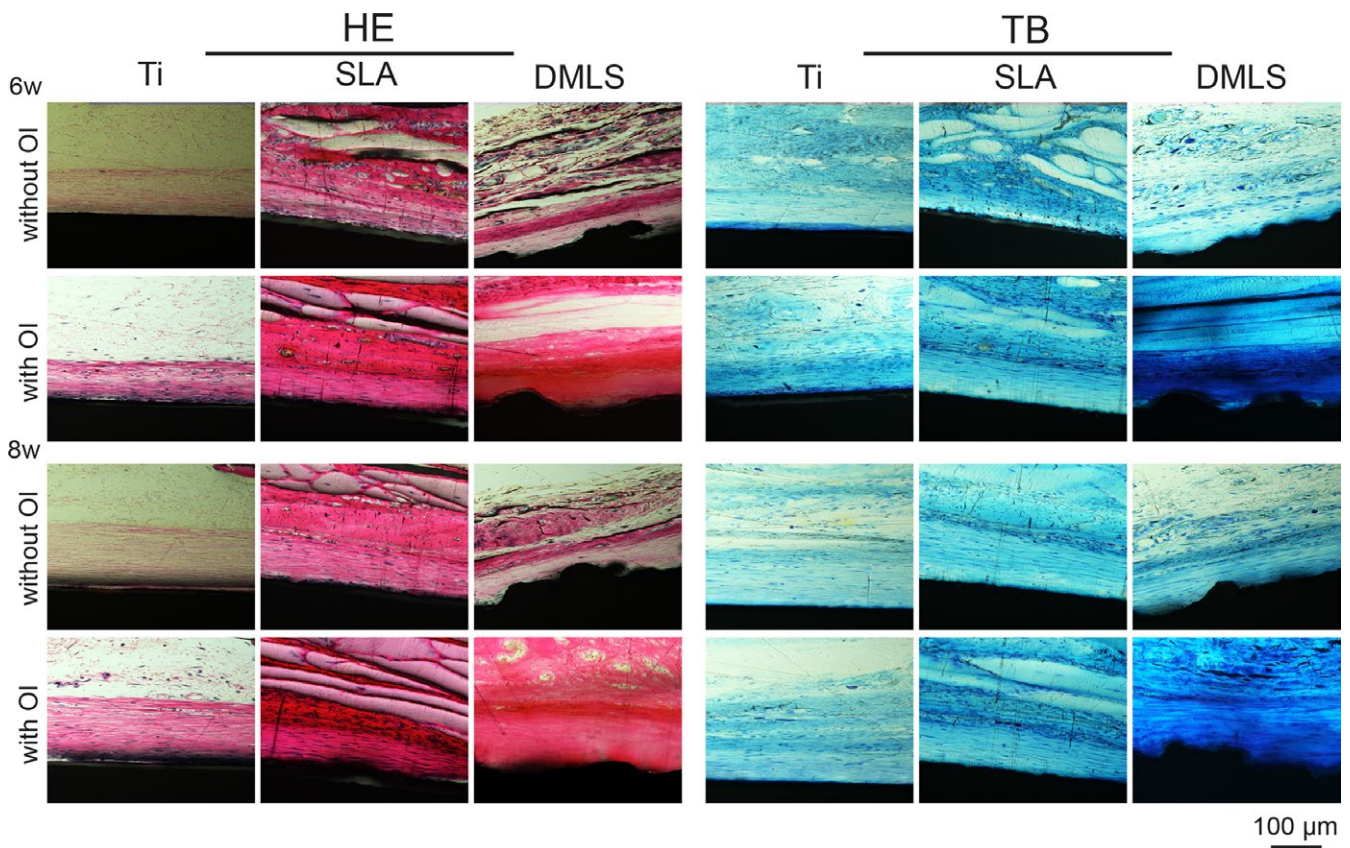
FIGURE 5 Ectopic bone formation. Haematoxylin and eosin (HE) and toluidine blue (TB) staining on the hard tissue slices, 6 and 8 weeks after the implantation of Ti, SLA and direct metal laser sintering (DMLS) titanium specimens
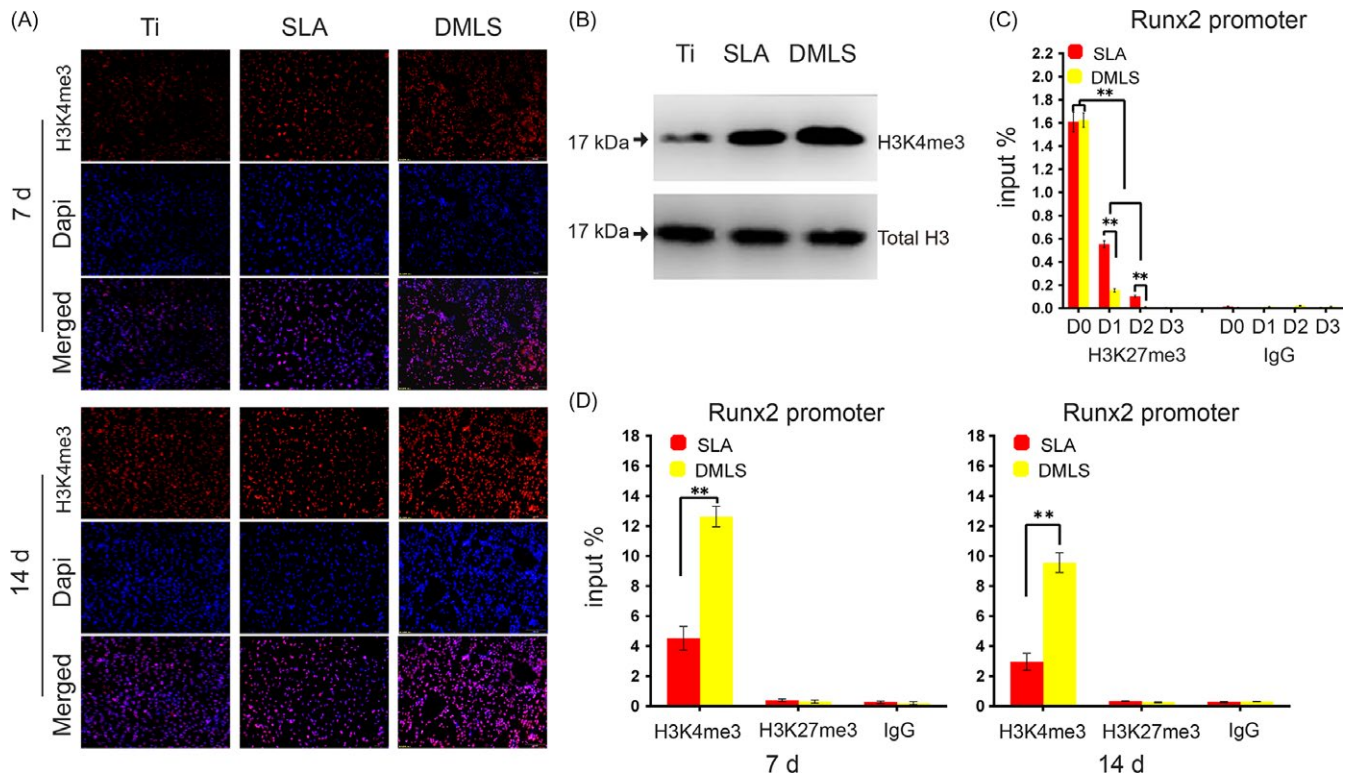
FIGURE 6 Epigenetic regulation of BMSCs on the direct metal laser sintering (DMLS) titanium surface. (A) Immunofluorescence staining for H3K4me3 in BMSCs (red, H3K4me3; blue, DAPI) cultured on Ti, SLA and DMLS titanium surfaces for 7 and 14 days. (B) Protein expression of H3K4me3 at day 14 after osteoinduction. (C) ChIP assay of the H3K27me3 level at the promoter area of the osteogenic gene *Runx2* at 0, 1, 2, 3 days. (D) ChIP assay of the H3K4me3 level at the promoter area of the osteogenic gene *Runx2* at 7 days and 14 days. Error bars represent SD (n = 3). **$P < .01$

onto the ridge/groove boundaries of microgrooved metallic surfaces. In this study, DMLS surface was found to be more hydrophilic, and its hierarchical micro/nanoscale topography exhibited greater protein adsorption ability than the SLA and Ti surfaces. Therefore, the DMLS surface was concluded to be favourable for cell adhesion, and it could also provide a better microenvironment to instruct stem cells to differentiate, which were unequivocally corroborated by the following results.

As illustrated by the SEM and CLSM analyses, cells on the DMLS surface exhibited faster adhesion and greater extension than those on SLA and Ti surfaces. One possible reason is that the hierarchical micro/nanoscale topography of DMLS surface could provide more protein binding sites to the integrins on the cell membrane, and in turn improve integrins clustering into focal adhesion complexes.[1,2,38] In addition, once a cell-material junction is established, unbundled actin-fibril-driven filopodia allow the cell to probe the surface structures.[39] During this process, F-actin bundles come into forming as response to the hierarchical topography, giving rise to larger finger-like filopodia.[39-41] As further F-actin polymerization is induced by the topographical cues,[39,42] sheet-like lamellipodia appear between the matured filopodia,[43] resulting in enhanced cell extension. In this study, attached cells on the DMLS surface exhibited a well-spread shape with more polygonal lamellipodia than those on SLA and Ti surfaces, verifying that hierarchical micro/nanoscale topography of

DMLS surface has greater capability to promote cell adhesion and pseudopodia extension.

Mediated by alterations in cell adhesion and extension, stem cells would further respond to surface topographical features with changes in cell proliferation and differentiation.[39] It has been reported that combined micro/nanoscale surface topography is more favourable than individual microscale topography for cell proliferation.[22,44] However, a debate emerged in response to data showing unfavourable cell proliferation on nanogroove or nanotube topography compared to that on smooth control.[45,46] According to our data, the hierarchical micro/nanoscale topography of DMLS surface seems to delay the emergence of the plateau phase rather than accelerate the rate of cell proliferation, thus increasing the cell number at maximal confluence. It was posited that a fine-tuned balance between proliferation and differentiation was achieved on DMLS surface, which would provide an ideal situation for bone growth and repair.[46]

For cell differentiation, previous studies on surfaces possessed both microscale roughness and a high density of nanoscale features showed that osteogenic differentiation was greatly enhanced.[22,23] That was confirmed by our results. In this study, cells cultured on the DMLS surfaces exhibited significantly higher *Runx2* and *OC* expression levels and higher ALP activity compared with those on SLA and Ti surfaces. Moreover, the total Runx2 protein level in the DMLS
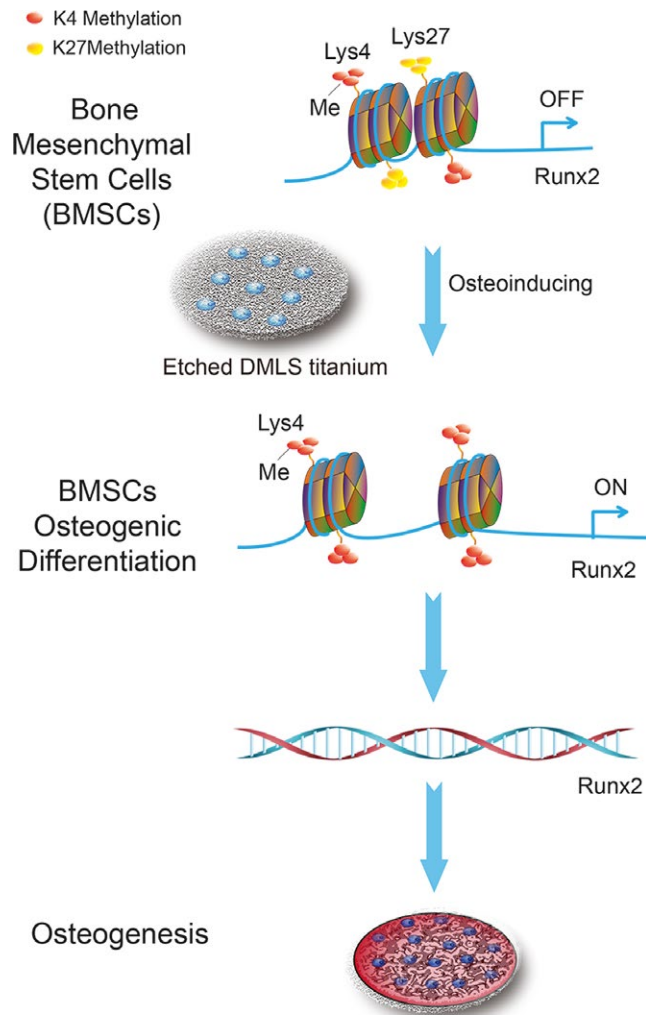
FIGURE 7 Schematic representation of the epigenetic regulation by the surface topography of direct metal laser sintering (DMLS) titanium to promote BMSC osteogenic differentiation

group was higher than that in the other groups. These results suggest that the hierarchical micro/nanoscale topography of DMLS surface provides a better microenvironment for the osteogenic differentiation of BMSCs than the other samples. Besides, nanotopographic cues have been reported to alter the organization of various cytoskeletal components (eg, F-actin, α-tubulin and γ-tubulin) and therefore affect cell morphology, with a tendency to favour osteogenic differentiation.[47,48] In this study, it was observed that cells on DMLS surface exhibited more F-actin in the cytoskeleton and larger bundles of filament compared with the Ti group. These results are consistent with the aforementioned studies. In addition, ectopic bone formation *in vivo* demonstrated obvious bone matrix formation on the DMLS surfaces, and the newly formed bone tissue invaded into the pore regions with no inflammatory reaction, indicating a great *in vivo* osteoinducing ability of the hierarchical micro/nanoscale topography. On the basis of verified ability of DMLS surface topographical cues to influence BMSC fate, an analysis of the underlying mechanisms was further explored in the subsequent experiments.

The nucleus is physically linked to the ECM and to other cells as part of a continuous cross-cell stretching network consisting of extracellular and intracellular fibres. Topographical features can affect focal adhesion assembly, intracellular actin polymerization and cell morphology. All these changes in turn alter the nuclear matrix through cytoskeletal filaments, through the recruitment of epigenetic modifiers or through reorganization of chromatin to control stem cell fates.[49-51] The understanding of the epigenetic regulatory mechanisms that are governed by topography cues and affect stem cell functions is still in the infant stage.[24,27,50] Since H3K4me3 and H3K27me3 are clearly associated with transcriptional activation or repression,[26] we measured the global level of H3K4me3 during the osteogenic differentiation process of BMSCs. Based on our results, a marked increase in H3K4me3 levels was detected in cells cultured on DMLS surfaces compared with those for SLA surfaces. Meanwhile, a ChIP assay was also performed to explore the histone modification dynamics at the promoter of the osteogenic gene *Runx2*. Interestingly, a bivalent state with co-occupancy by the H3K4me3 and H3K27me3 markers was observed at the *Runx2* promoter in BMSCs before the induction of differentiation. Bivalent domains were first described in embryonic stem cells (ESCs) and were postulated to prepare developmental regulatory genes for later transcriptional activation upon differentiation.[52] For ESCs, to maintain self-renewal, the promoter of various key developmental genes is marked by H3K27me3 and these promoters often carry the activating H3K4 mark as well. At the end of ESC lineage commitment, these bivalent domains have been resolved to carry either activating (H3K4me3) or inactivating (H3K27me3) marks in a lineage-specific manner.[53] Our results also showed the osteogenesis-associated gene expression in BMSCs is efficiently induced by a rapid H3K27 demethylation and increase in H3K4me3 levels at gene promoters upon osteogenic differentiation on DMLS titanium surface. Therefore, topographical cues of DMLS surface likely contribute to the resolution of the bivalent state of osteogenic genes, facilitating the osteogenic differentiation of BMSCs.

Together, DMLS implant surfaces with hierarchical micro/nanoscale topography have greater potential for the induction of osteogenic differentiation of BMSCs both *in vitro* and *in vivo* than SLA and Ti surfaces. And we demonstrate a potential epigenetic mechanism: the appropriate topography allows rapid H3K27 demethylation and an increased H3K4me3 level at the promoter region of osteogenesis-associated genes during the osteogenic differentiation of BMSCs (Figure 7).

For the first time, we explored the effect of DMLS surfaces with hierarchical micro/nanoscale topography on cell behaviour from the aspect of epigenetic regulation. However, epigenetic regulation of stem cell lineage commitment is extensive and complex. Due to technical limitations, uncovering the epigenetic mechanisms by which surface topography directs stem cell fates is still a significant challenge. In the future, systematic examination of epigenomic changes by high throughput ChIP sequencing in response to the topographical cues of material surfaces could provide new insights that would aid implant surface modification and improve bone tissue engineering.

CONFLICT OF INTEREST

The authors declare that they have no conflict of interest.

AUTHORS' CONTRIBUTIONS

All the authors were involved in the work. X.Z., X.W. and L.S. conceived the idea of the study. G.Z., B.G. and X.Q. fabricated and characterized the materials. G.Z., B.G. and P.H. designed and performed the experiments. Z.L. and R.L. helped with the animal experiments. P.W. and P.G. provided financial support. G.Z. and Y.K. analysed the data.

ORCID

Xudong Wu http://orcid.org/0000-0001-9594-479X

Lei Sui http://orcid.org/0000-0003-3586-9999

REFERENCES

1. Griffin M, Butler PE, Seifalian AM, Kalaskar DM. Control of stem cell fate by engineering their micro and nanoenvironment. *World J Stem Cells*. 2015;7:37-50.
2. Guilak F, Cohen DM, Estes BT, Gimble JM, Liedtke W, Chen CS. Control of stem cell fate by physical interactions with the extracellular matrix. *Cell Stem Cell*. 2009;5:17-26.
3. Lutolf MP, Gilbert PM, Blau HM. Designing materials to direct stem-cell fate. *Nature*. 2009;462:433-441.
4. Cha C, Liechty WB, Khademhosseini A, Peppas NA. Designing biomaterials to direct stem cell fate. *ACS Nano*. 2012;6: 9353-9358.
5. Ventre M, Netti PA. Engineering cell instructive materials to control cell fate and functions through material cues and surface patterning. *ACS Appl Mater Interfaces*. 2016;8:14896-14908.
6. Prabhakaran MP, Vatankhah E, Kai D, Ramakrishna S. Methods for nano/micropatterning of substrates: toward stem cells differentiation. *Int J Polym Mater*. 2015;64:338-353.
7. Rovensky YA. *Topographic Cell Responses. Adhesive Interactions in Normal and Transformed Cells*. New York: Springer Science; 2011:153-184.
8. Liao S, Nguyen LT, Ngiam M, et al. Biomimetic nanocomposites to control osteogenic differentiation of human mesenchymal stem cells. *Adv Healthc Mater*. 2014;3:737-751.
9. Dimitrievska S, Bureau M, Antoniou J, et al. Titania-hydroxyapatite nanocomposite coatings support human mesenchymal stem cells osteogenic differentiation. *J Biomed Mater Res, Part A*. 2011;98:576-588.
10. Yang W, Han W, He W, et al. Surface topography of hydroxyapatite promotes osteogenic differentiation of human bone marrow mesenchymal stem cells. *Mater Sci Eng C*. 2016;60:45-53.
11. Abagnale G, Steger M, Nguyen VH, et al. Surface topography enhances differentiation of mesenchymal stem cells towards osteogenic and adipogenic lineages. *Biomaterials*. 2015;61:316-326.
12. Hollander DA, Von Walter M, Wirtz T, et al. Structural, mechanical and in vitro characterization of individually structured Ti–6Al–4V produced by direct laser forming. *Biomaterials*. 2006;27:955-963.
13. Rho J, Kuhnspearing L, Zioupos P. Mechanical properties and the hierarchical structure of bone. *Med Eng Phys*. 1998;20:92-102.
14. Stevens MM, George JH. Exploring and engineering the cell surface interface. *Science*. 2005;310:1135-1138.
15. Oftadeh R, Perezviloria M, Villacamacho JC, Vaziri A, Nazarian A. Biomechanics and mechanobiology of trabecular bone: a review. *J Biomech Eng-T Asme*. 2015;137:010802.
16. Mendonca G, Mendonca DBS, Aragao FJL, Cooper LF. Advancing dental implant surface technology–from micron- to nanotopography. *Biomaterials*. 2008;29:3822-3835.
17. Ruckh TT, Porter JR, Allam NK, Feng X, Grimes CA, Popat KC. Nanostructured tantala as a template for enhanced osseointegration. *Nanotechnology*. 2009;20:045102.
18. Zhao L, Liu L, Wu Z, Zhang Y, Chu PK. Effects of micropitted/nanotubular titania topographies on bone mesenchymal stem cell osteogenic differentiation. *Biomaterials*. 2012;33:2629-2641.
19. Zhang J, Luo X, Barbieri D, et al. The size of surface microstructures as an osteogenic factor in calcium phosphate ceramics. *Acta Biomater*. 2014;10:3254-3263.
20. Lai M, Cai K, Hu Y, Yang X, Liu Q. Regulation of the behaviors of mesenchymal stem cells by surface nanostructured titanium. *Colloids Surf, B*. 2012;97:211-220.
21. Gittens RA, Olivaresnavarrete R, Mclachlan T, et al. Differential responses of osteoblast lineage cells to nanotopographically-modified microroughened titanium-aluminum-vanadium alloy surfaces. *Biomaterials*. 2012;33:8986-8994.
22. Kubo K, Tsukimura N, Iwasa F, et al. Cellular behavior on TiO2 nanonodular structures in a micro-to-nanoscale hierarchy model. *Biomaterials*. 2009;30:5319-5329.
23. Xie Y, Ao H, Xin S, Zheng X, Ding C. Enhanced cellular responses to titanium coating with hierarchical hybrid structure. *Mat Sci Eng C*. 2014;38:272-277.
24. Li Y, Chu J, Kurpinski K, et al. Biophysical regulation of histone acetylation in mesenchymal stem cells. *Biophys J* . 2011;100:1902-1909.
25. Fullgrabe J, Hajji N, Joseph B. Cracking the death code: apoptosis-related histone modifications. *Cell Death Differ*. 2010;17:1238-1243.
26. Voigt P, Tee W-W, Reinberg D. A double take on bivalent promoters. *Genes Dev*. 2013;27:1318-1338.
27. Morez C, Noseda M, Paiva M, Belian E, Schneider MD, Stevens MM. Enhanced efficiency of genetic programming toward cardiomyocyte creation through topographical cues. *Biomaterials*. 2015;70:94-104.
28. Ge WS, Shi L, Zhou Y, et al. Inhibition of osteogenic differentiation of human adipose-derived stromal cells by retinoblastoma binding protein 2 repression of RUNX2-activated transcription. *Stem Cells*. 2011;29:1112-1125.
29. Dahl JA, Collas P. A rapid micro chromatin immunoprecipitation assay (ChIP). *Nat Protoc*. 2008;3:1032-1045.
30. Zhang J, Ma X, Lin D, et al. Magnesium modification of a calcium phosphate cement alters bone marrow stromal cell behavior via an integrin-mediated mechanism. *Biomaterials*. 2015;53:251-264.
31. Khang D, Kim SY, Liusnyder P, Palmore GTR, Durbin SM, Webster TJ. Enhanced fibronectin adsorption on carbon nanotube/poly(carbonate) urethane: independent role of surface nano-roughness and associated surface energy. *Biomaterials*. 2007;28:4756-4768.

32. Dolatshahi-Pirouz A, Jensen T, Kraft DC, et al. Fibronectin adsorption, cell adhesion, and proliferation on nanostructured tantalum surfaces. *ACS Nano*. 2010;4:2874-2882.

33. Karakeçili A, Messina GM, Yurtsever MÇ, Gümüşderelioğlu M, Marletta G. Impact of selective fibronectin nanoconfinement on human dental pulp stem cells. *Colloids Surf, B*. 2014;123:39-48.

34. Brammer KS, Frandsen CJ, Jin S. TiO2 nanotubes for bone regeneration. *Trends Biotechnol*. 2012;30:315-322.

35. Mcmahon R, Wang L, Skoracki RJ, Mathur AB. Development of nanomaterials for bone repair and regeneration. *J Biomed Mater Res B*. 2013;101:387-397.

36. Ko Y, Lee K, Kim B. Effect of functional groups on biodegradation and pre-osteoblastic cell response on the plasma-polymerized magnesium surface. *Jpn J Appl Phys*. 2013;52:20-21.

37. De Luca AC, Zink M, Weidt A, Mayr SG, Markaki AE. Effect of microgrooved surface topography on osteoblast maturation and protein adsorption. *J Biomed Mater Res*, Part A. 2015;103:2689-2700.

38. Khang D, Choi J, Im Y, et al. Role of subnano-, nano- and submicron-surface features on osteoblast differentiation of bone marrow mesenchymal stem cells. *Biomaterials*. 2012;33:5997-6007.

39. Dalby M, Gadegaard N, Oreffo R. Harnessing nanotopography and integrin-matrix interactions to influence stem cell fate. *Nat Mater*. 2014;13:558-569.

40. Berrier AL, Yamada KM. Cell–matrix adhesion. *J Cell Physiol*. 2007;213:565-573.

41. Hynes RO. Integrins: bidirectional, allosteric signaling machines. *Cell*. 2002;110:673-687.

42. Seo CH, Jeong H, Feng Y, et al. Micropit surfaces designed for accelerating osteogenic differentiation of murine mesenchymal stem cells via enhancing focal adhesion and actin polymerization. *Biomaterials*. 2014;35:2245-2252.

43. Ballestrem C, Wehrlehaller B, Hinz B, Imhof BA. Actin-dependent lamellipodia formation and microtubule-dependent tail retraction control-directed cell migration. *Mol Biol Cell*. 2000;11:2999-3012.

44. Zhao L, Mei S, Chu PK, Zhang Y, Wu Z. The influence of hierarchical hybrid micro/nano-textured titanium surface with titania nanotubes on osteoblast functions. *Biomaterials*. 2010;31:5072-5082.

45. Wang P, Thissen H, Kingshott P. Modulation of human multipotent and pluripotent stem cells using surface nanotopographies and surface-immobilised bioactive signals: a review. *Acta Biomater*. 2016;45:31-59.

46. Gittens RA, Mclachlan T, Olivaresnavarrete R, et al. The effects of combined micron-/submicron-scale surface roughness and nanoscale features on cell proliferation and differentiation. *Biomaterials*. 2011;32:3395-3403.

47. Gerecht S, Bettinger CJ, Zhang Z, Borenstein JT, Vunjaknovakovic G, Langer R. The effect of actin disrupting agents on contact guidance of human embryonic stem cells. *Biomaterials*. 2007;28:4068-4077.

48. Hsieh W, Liu Y, Lee Y, Rimando MG, Lin K, Lee OK. Matrix dimensionality and stiffness cooperatively regulate osteogenesis of mesenchymal stromal cells. *Acta Biomater*. 2016;32:210-222.

49. Wang N, Tytell JD, Ingber DE. Mechanotransduction at a distance: mechanically coupling the extracellular matrix with the nucleus. *Nat Rev Mol Cell Biol*. 2009;10:75-82.

50. Crowder SW, Leonardo V, Whittaker T, Papathanasiou P, Stevens MM. Material cues as potent regulators of epigenetics and stem cell function. *Cell Stem Cell*. 2016;18:39-52.

51. Pablo Rodríguez J, González M, Ríos S, Cambiazo V. Cytoskeletal organization of human mesenchymal stem cells (MSC) changes during their osteogenic differentiation. *J Cell Biochem*. 2004;93:721-731.

52. Liu X, Wang C, Liu W, et al. Distinct features of H3K4me3 and H3K27me3 chromatin domains in pre-implantation embryos. *Nature*. 2016;537:558-562.

53. Bernstein BE, Mikkelsen TS, Xie X, et al. A bivalent chromatin structure marks key developmental genes in embryonic stem cells. *Cell*. 2006;125:315-326.